

Research



Cite this article: Kaurin D, Bal PK, Arroyo M. 2022 Peeling dynamics of fluid membranes bridged by molecular bonds: moving or breaking. *J. R. Soc. Interface* **19**: 20220183. <https://doi.org/10.1098/rsif.2022.0183>

Received: 7 March 2022

Accepted: 1 June 2022

Subject Category:

Life Sciences—Physics interface

Subject Areas:

biomechanics, biophysics, biomaterials

Keywords:

cell–cell adhesion, peeling, vesicle adhesion

Author for correspondence:

Marino Arroyo

e-mail: marino.arroyo@upc.edu

Electronic supplementary material is available online at <https://doi.org/10.6084/m9.figshare.c.6039045>.

Peeling dynamics of fluid membranes bridged by molecular bonds: moving or breaking

Dimitri Kaurin¹, Pradeep K. Bal¹ and Marino Arroyo^{1,2,3}

¹Universitat Politècnica de Catalunya-BarcelonaTech, 08034 Barcelona, Spain

²Institute for Bioengineering of Catalonia (IBEC), The Barcelona Institute of Science and Technology, 08034 Barcelona, Spain

³CIMNE, 08034 Barcelona, Spain

PKB, 0000-0001-7408-0996; MA, 0000-0003-1647-940X

Biological adhesion is a critical mechanical function of complex organisms. At the scale of cell–cell contacts, adhesion is remarkably tunable to enable both cohesion and malleability during development, homeostasis and disease. It is physically supported by transient and laterally mobile molecular bonds embedded in fluid membranes. Thus, unlike specific adhesion at solid–solid or solid–fluid interfaces, peeling at fluid–fluid interfaces can proceed by breaking bonds, by moving bonds or by a combination of both. How the additional degree of freedom provided by bond mobility changes the mechanics of peeling is not understood. To address this, we develop a theoretical model coupling diffusion, reactions and mechanics. Mobility and reaction rates determine distinct peeling regimes. In a diffusion-dominated Stefan-like regime, bond motion establishes self-stabilizing dynamics that increase the effective fracture energy. In a reaction-dominated regime, peeling proceeds by travelling fronts where marginal diffusion and unbinding control peeling speed. In a mixed reaction–diffusion regime, strengthening by bond motion competes with weakening by bond breaking in a force-dependent manner, defining the strength of the adhesion patch. In turn, patch strength depends on molecular properties such as bond stiffness, force sensitivity or crowding. We thus establish the physical rules enabling tunable cohesion in cellular tissues and in engineered biomimetic systems.

1. Introduction

Cell–cell adhesion is an essential mechanical function that is required to maintain tissue integrity under mechanical stress [1–3], disrupted during cancer [4] and finely tuned during development [5–7] or wound healing [8]. Cell–cell adhesion needs to manage a contradiction between stability and malleability. Such versatile and adaptable interfaces avoid unspecific adhesion [9], and instead rely on the collective effect of weak transmembrane bonds, notably of the cadherin family [10]. Cell–cell adhesion is a multi-scale and highly regulated function that involves bond clustering, coupling to the cytoskeleton through mechanosensitive adapter proteins, turnover through endocytosis [11,12] and Ca²⁺-mediated control of the molecular properties of the binders and bonds, including diffusivity [10,13], stiffness [13] and force sensitivity [14]. The distinguishing physical feature of cell–cell adhesion as compared with cell–matrix adhesion, and in general compared with conventional specific adhesion at solid–solid or solid–fluid interfaces, is that both free binders and bonds are embedded in fluid membranes and hence are laterally mobile. As a result, the dynamics of adhesion between cells, and more generally between fluid membranes bridged by transient bonds, depend on binding/unbinding reactions between partner molecules and on the lateral motion of bonds and

free binders. Despite this fact being long acknowledged [9,15–17], its consequences for the dynamics of peeling are not understood and a mapping of the different dynamical scenarios of decohesion is lacking.

To isolate the physical aspects of cell–cell adhesion, previous studies have focused on minimal artificial models based on lipid membranes decorated with adhesion molecules [18–24]. While the theoretical understanding of equilibrium in such systems is established [9,25], adhesion dynamics under force have been barely studied theoretically even though the mechanical environment of cell–cell adhesions is fundamentally dynamical. Here, we focus on the dynamics of unbinding of two vesicles held together by an adhesive patch made of mobile adhesion molecules forming transient *trans* bonds. Our model is also pertinent to the forced unbinding of adjacent cells, since adhesion molecules attached to the cortex are still mobile owing to the turnover of cortical components.

During peeling, an adhesion patch shrinks, possibly until complete separation. In a tear-out limiting scenario, shrinkage of the patch may proceed by sequential bond breaking [15,16,26–30]. When a vesicle with mobile binders adheres to a substrate with fixed receptors, spreading critically depends on diffusion of free binders on the vesicle [31–33]; however, for immobile bonds, peeling necessarily proceeds by tear-out. Peeling by bond breaking has been extensively studied theoretically [15,34–36]. In a competing limiting scenario, the patch may shrink by lateral motion of bonds leading to an increasingly crowded patch [16,17], a situation observed during cell–cell separation *in vitro* and in developing embryos [7,37–39]. In general, the dynamics of decohesion may depend on a combination of bond breaking and bond motion (or reaction and diffusion), but this interplay has not been systematically examined [15,16,27,40] despite the fact that bond mobility has been shown to strongly influence adhesions in hybrid cell-supported bilayer studies [41] and in purely artificial systems [21].

To understand the physical principles governing peeling of an adhesive interface bridged by mobile bonds, we develop a self-consistent continuum dynamical model capturing the reaction kinetics of bond formation and dissociation, the lateral diffusion of adhesion molecules and the mechanics of the adhesion patch and of the adhering vesicles. We then identify and characterize distinct regimes pertinent to (i) long-lived mobile bonds, (ii) short-lived bonds with reduced mobility such as cadherin molecules linked to the cell cytoskeleton, and (iii) short-lived mobile bonds such as cadherins in a lipid bilayer. Each of these regimes exhibits fundamentally different dynamics (self-similar, travelling or multiphase) with multi-scale features in space and time. We further examine the relation between molecular properties of bonds and the effective behaviour of the adhesive patch.

2. Methods

2.1. Theoretical and computational model

The state of the system is defined by the shape of the adhering vesicles and the number concentration of bonds on the adhesion patch, c_1 , and that of free binders on the entire vesicle, c_2 . We assume that the adhering vesicles are identical and are made of a fluid membrane where bonds and free binders are mobile. Focusing first on a dilute limit and non-compliant bonds, the

chemical potentials of bonds and free binders take the form $\mu_i = \mu_i^0 + k_B T \log c_i/c_0$, $i = 1, 2$, where μ_i^0 is the standard chemical potential, $k_B T$ is the thermal energy scale and c_0 is an arbitrary reference concentration; see [42] for a detailed equilibrium statistical mechanics treatment. In equilibrium, shape and concentrations obey chemical and mechanical equilibrium conditions [25]. Chemical equilibrium requires that μ_1 (and hence c_1) is uniform on the adhesion patch, that μ_2 (and hence c_2) is uniform on the entire vesicle including the adhesion patch and that $\mu_1 = 2\mu_2$ over the patch since two free binders react to form a bond. This last condition implies that

$$\bar{K} = c_0 c_1 / c_2^2 = \exp \left[\frac{2\mu_2^0 - \mu_1^0}{k_B T} \right], \quad (2.1)$$

with \bar{K} the non-dimensional equilibrium constant of the binders in the two-dimensional environment of the adhesion patch [43], further discussed below. At high membrane tension γ expected for a mature adhesion patch rich in bonds, the length scale $\ell_1 = \sqrt{\kappa/\gamma}$, where $\kappa \sim 10^{-19}$ J is the bending stiffness, is much smaller than the vesicle size. In this capillary limit, mechanical equilibrium at the edge of the adhesion patch is formally a Young–Dupré equation, $k_B T c_1 = 2\gamma(1 - \cos\theta)$, where the left-hand side is the dilute approximation of the osmotic tension of the bonds in the adhesion patch and θ is the contact angle between the free part of the vesicle and the symmetry plane [17,25] (figure 1a). Being commensurate with the osmotic tension of bonds, we estimate membrane tension for a typical bond concentration of $c_1 \sim 4 \times 10^3$ molecules/ μm^2 to be $\gamma \sim 1.6 \times 10^{-5}$ N m $^{-1}$ and hence $\ell_1 \sim 70$ nm. With the precise parameters considered in our examples below, ℓ_1 is close to 20 nm. Besides justifying the capillary limit, high tension suppresses thermal fluctuations of the membrane [44,45], which are not considered here but play a prominent role during low-tension adhesion spreading [21,24]. Mechanical equilibrium in the non-adhered part of the vesicle is expressed by Laplace’s law. These conditions determine the equilibrium shape of the vesicles, the size of the adhesion and the concentration of free binders and bonds.

Describing the out-of-equilibrium dynamics under force requires accounting for diffusion and chemical kinetics, which in turn depend on mechanics in different ways. Diffusion of bonds is biased by their tendency to leave regions where they are highly stretched. Chemical kinetics are influenced by mechanics since unbinding rates are force sensitive and rebinding rates depend on the distance between potential partners [34,36]. We thus need to resolve the force borne by bonds and the separation between membranes required to compute these rates. However, a single mechanical modelling resolving simultaneously the vesicle-scale capillary mechanics at length scales of tens of micrometres and the separation profile near the edge of the adhesion patch with sub-nanometre resolution is very challenging from a computational point of view. For this reason, exploiting scale separation, we combine a vesicle-scale capillary model in terms of macroscopic quantities such as patch size, contact angle or vesicle pressure with a model for the micro-mechanics of the adhesion patch, taking the macroscopic quantities as parameters and resolving the force on bonds by accounting for the bending rigidity of the membrane κ and the compliance of the molecular bonds (figure 1c,d). In this model, the length scale over which the tension of the free-standing membrane is transmitted to the adhesion patch can be estimated by balancing the bending and the bond normal pressures as $\ell_2 = \sqrt{[4]\kappa/(kc_1)}$ [46], where k is the bond stiffness and c_1 is a typical bond concentration. Considering $k = 2.5 \times 10^{-4}$ N m $^{-1}$ and the values given above for κ and c_1 , we find that $\ell_2 \sim 20$ nm, much smaller than the typical size of an adhesion patch.

To focus on the mechano-chemistry of forced decohesion and to simplify all other aspects of the model, we restrict ourselves to a two-dimensional geometry where the membrane

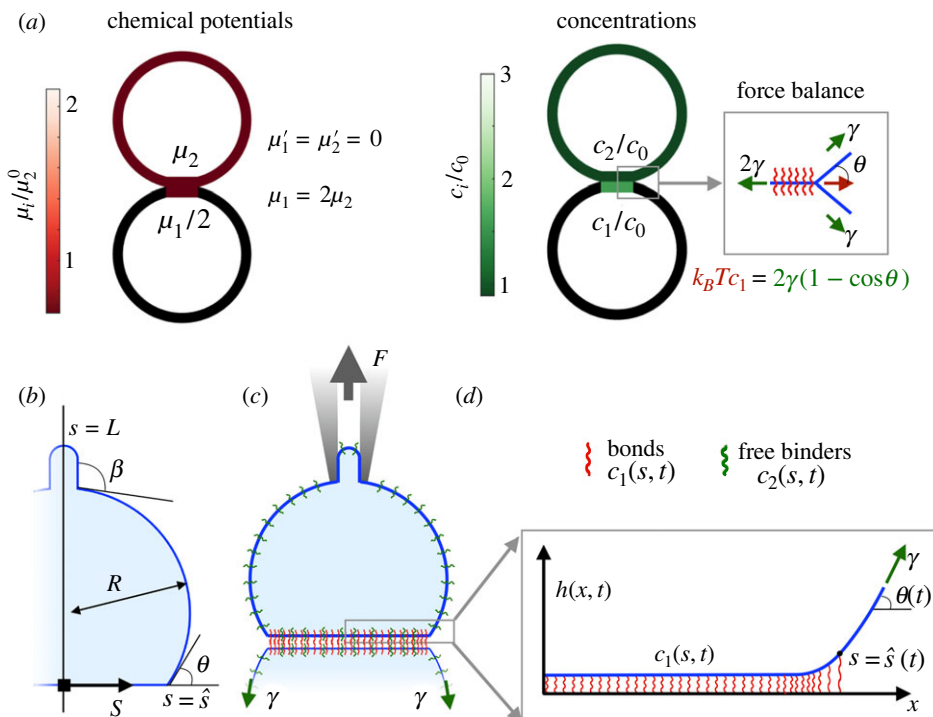


Figure 1. (a) Equilibrium of two identical vesicles adhering through mobile non-compliant binders. Chemical equilibrium requires uniformity and equality of the chemical potentials (left). Mechanical equilibrium requires satisfaction of the Young–Laplace and Young–Dupré relations (right). (b) A capillary model describing membrane mechanics in terms of the half-size of the adhesion \hat{s} , the angles θ and β and the radius R . (c) A schematic of the system, where a loading device controls surface tension γ and force F . (d) Micro-mechanics model of the adhesion patch resolving the separation profile relative to an equilibrium separation h , accounting for bending stiffness and bond compliance.

becomes a line whose arc-length coordinate is denoted by s . We summarize here the theoretical model and provide a detailed derivation based on Onsager’s variational formalism in electronic supplementary material, note 1. The vesicle is connected to a loading device, which controls membrane tension γ by drawing or supplying membrane length (area in three dimensions) and applies a vertical force F (figure 1c). The area enclosed by the curve defining the two-dimensional vesicle is kept constant by a pressure difference P . The mechanical ensemble thus simulates in two dimensions a vesicle whose enclosed volume is constant and which is aspirated by a micropipette that controls membrane tension [37–39]. Mechanical relaxation is much faster than chemical relaxation, and thus we treat the mechanics quasi-statically. Given the prescribed γ and F and the current size of the adhesion patch $\hat{s}(t)$, the capillary model provides the shape of the vesicle (figure 1b), in particular the contact angle θ and the pressure P . With this information and the current concentration of bonds $c_1(s, t)$, the micro-mechanical model provides the membrane separation profile $h(x, t)$ (figure 1d), by minimizing the functional capturing the mechanics of the adhesive patch

$$\tilde{\mathcal{F}}[h] = \gamma \int_0^{\alpha \hat{s}} \sqrt{1 + h'^2} dx + \frac{\kappa}{2} \int_0^{\alpha \hat{s}} \frac{h''^2}{(1 + h'^2)^{5/2}} dx + \int_0^{\hat{s}} \frac{\kappa c_1}{2} h^2 dx + \int_0^{\hat{s}} P h dx - \gamma \sin \theta h(\alpha \hat{s}). \quad (2.2)$$

The first term is a capillary energy and results from $ds = \sqrt{1 + h'^2} dx$. The second term is then bending energy, since the curvature of the curve can be written as $h''/(1 + h'^2)^{3/2}$. The third term is the energy stored in the elastic foundation, whose stiffness is given by the number concentration of bound binders c_1 multiplied by the stiffness to stretching of one bond, k . The fourth term accounts for the pressure inside the vesicle, which presses against the molecular bonds. The last term is the potential energy of the tension force at the boundary of the

domain. $\alpha > 1$ is a parameter such that $(\alpha - 1)\hat{s} > \ell_1$, and hence the boundary of the micro-mechanical model in the top-right of figure 1d is not affected by bending elasticity and the results are insensitive to this parameter. Minimization of equation (2.2) allows us to compute the out-of-plane force per molecule $k h(s, t)$ within the patch region. In turn, this information allows us to evolve the bond and free-binder concentrations $c_1(s, t)$ and $c_2(s, t)$ and the position of the interface $\hat{s}(t)$ as discussed next.

The reaction–diffusion dynamics for c_1 and c_2 are given by

$$\dot{c}_1 = D_1 \left[c_1' + c_1 \left(\frac{h^2}{x_\gamma^2} \right)' \right] + k_{\text{on}} c_2 - k_{\text{off}} c_1 \quad \text{in } (0, \hat{s}(t)), \quad (2.3)$$

$$\dot{c}_2 = D_2 c_2'' - k_{\text{on}} c_2 + k_{\text{off}} c_1 \quad \text{in } (0, \hat{s}(t)) \quad (2.4)$$

$$\text{and} \quad \dot{c}_2 = D_2 c_2'' \quad \text{in } (\hat{s}(t), L_0), \quad (2.5)$$

where dots and primes denote time and space derivatives, $D_{1,2}$ are diffusion constants of bonds/free binders, k_{on} is the binding rate, k_{off} is the unbinding rate, L_0 is the total membrane length and $x_\gamma = \sqrt{k_B T/k}$ is the scale of thermal fluctuations of binders. These partial differential equations are defined on a time-dependent domain. The transport term in equation (2.3) includes a diffusive term and a bias, according to which bonds try to reduce the mechanical contribution of their chemical potential [9,40],

$$\mu_1(c_1, h) = \mu_1^0 + k_B T \log \frac{c_1}{c_0} + k_B T \left(\frac{h}{x_\gamma} \right)^2, \quad (2.6)$$

by moving away from regions where they are highly stretched. An additional consequence of the stretching term in the chemical potential of bonds identified by our model is the dependence of the binding rate on separation, in agreement with previous treatments [9,34,36]

$$k_{\text{on}}(h) = \bar{k}_{\text{on}} \exp \left[- \left(\frac{h}{x_\gamma} \right)^2 \right], \quad (2.7)$$

where \bar{k}_{on} is the reference binding rate for $h=0$. This expression captures the fact that the probability of bond formation depends on the proximity of potential partners as they thermally fluctuate. By equating $\mu_1(c_1, h)$ in equation (2.6) with twice the chemical potential of free binders, $\mu_2(c_2) = \mu_2^0 + k_B T \log c_2/c_0$, we can identify a separation-dependent two-dimensional equilibrium constant $K(h) = \bar{K} \exp[-(h/x_\gamma)^2]$, where \bar{K} is given by equation (2.1). Interestingly, previous theories accounting for orientational entropy and membrane thermal fluctuations but not for bond extensional compliance have related three-dimensional to two-dimensional equilibrium constants to find the same dependence of $K(h)$ on separation with a different interpretation for x_γ [43,47]. In the present setting of high tension and forced peeling, membrane fluctuations may not be as important as bond deformability, but in general one can expect that the effective compliance of the binding domain depends on both the intrinsic compliance of the adhesion molecule and that of the membrane supporting the bond, which for adhesion molecules attached to the actin cortex includes adaptor molecules and the actin network. This suggests that x_γ , or alternatively k , should be regarded as an effective parameter rather than one strictly describing the stiffness of an adhesion molecule.

Although cadherin bonds are thought to shift between ideal, slip or catch bonds depending on environmental conditions and conformation [14,48], here we only consider the slip-bond behaviour as described by Bell's model [49]

$$k_{\text{off}}(h) = \bar{k}_{\text{off}} \exp\left(\frac{kh}{f_\beta}\right) = \bar{k}_{\text{off}} \exp\left(\frac{h}{x_\beta}\right), \quad (2.8)$$

where f_β is the force sensitivity and where we introduce a separation sensitivity $x_\beta = f_\beta/k$ for convenience.

The governing equations (2.3)–(2.5) need to be supplemented by initial, boundary and interface conditions at $s = \hat{s}(t)$. Since free binders can cross the interface, their concentration and flux are continuous. By contrast, the interface is by definition a barrier for bonds. Consequently, the diffusive flux of bonds at the interface must be compensated by bond transport owing to interface motion,

$$-D_1 \left\{ c_1' + c_1 \left[\left(\frac{h}{x_\gamma} \right)^2 \right]' \right\}_{s=\hat{s}} = c_1(\hat{s}, t) \hat{v}, \quad (2.9)$$

where $\hat{v} = d\hat{s}/dt$ is the velocity of the interface. Finally, force balance at the interface requires that

$$k_B T c_1(\hat{s}, t) = 2\gamma(1 - \cos \theta), \quad (2.10)$$

where now c_1 depends on space and time and is governed by equation (2.3). Comparison of this equation with Rivlin's classical theory of peeling [50] shows that osmotic tension of bonds at the interface, $k_B T c_1(\hat{s}, t)$, plays the role of the adhesion fracture energy. However, rather than a material property of the interface as in classical peeling and in the case of tear-out of a vesicle against a substrate with immobile receptors [17], here this quantity is a dynamical variable. Equations (2.3), (2.4), (2.9) and (2.10) supplemented by the initial and boundary conditions at $s=0$ and $s=L_0$ allow us to solve for $c_1(s, t)$, $c_2(s, t)$ and $\hat{s}(t)$. As these variables evolve, we need to update the mechanical variables θ and $h(s, t)$, which in turn affect the reaction–diffusion interface dynamics. The self-consistent finite-element numerical solution of the model is described in detail in electronic supplementary material, note 1.

2.2. System preparation and parameters

Before driving the system out of equilibrium, we prepared the system at an equilibrium state for non-compliant and ideal bonds. In all calculations, we set $\bar{K} = c_0 \bar{k}_{\text{on}}/\bar{k}_{\text{off}} = 2$, $F=0$, the vesicle radius to $R_0 = 10 \mu\text{m}$, $\hat{s}_0 = 2.5 \mu\text{m}$,

$c_0 = 2.5 \times 10^3 \text{ molecules}/\mu\text{m}^2 \times \ell_{\text{lat}}$, and the length of the half vesicle to $L_0 = 35 \mu\text{m}$. Thus, the total number of molecules is $N_{\text{tot}} = c_0 \times L_0$. Here, ℓ_{lat} is an arbitrary depth of our one-dimensional membrane to make it a ribbon, allowing us to map two-dimensional to one-dimensional number densities. Without loss of generality, $\mu_1^0 = 0$ and, from equation (2.1), we conclude that $\mu_2^0 = (k_B T \log \bar{K})/2$. In all figures, we non-dimensionalize chemical potentials by μ_2^0 . With these data, conservation of the total number of molecules, $N_{\text{tot}} = c_1 \hat{s}_0 + c_2 L_0$, and the law of mass action, $c_0 c_1/c_2^2 = \bar{K}$, provide two equations to solve for the equilibrium concentrations, obtaining $c_1 = 1.58 c_0$ and $c_2 = 0.89 c_0$. Since R_0 and \hat{s}_0 determine the contact angle as $\sin \theta_0 = \hat{s}_0/R_0$, the force balance at the interface provides an equation for the membrane tension, for which, taking $k_B T = 4.11 \times 10^{-21} \text{ J}$, we find $\gamma = 2.55 \times 10^{-4} \text{ N m}^{-1} \times \ell_{\text{lat}}$. This equilibrium state is illustrated in figure 1a.

Starting from this state and driving it out of equilibrium by suddenly increasing the applied force F , we tracked the mechano-chemical dynamics of forced decohesion, which tend to uniformize μ_1 and μ_2 over the patch and vesicle, and tend to equilibrate them as $\mu_1 = 2\mu_2$ over the patch. The time scale of bond diffusion in the adhesion patch is $\tau_{\text{diff},1} = \hat{s}_0^2/D_1$, whereas that of free binders on the entire vesicle is $\tau_{\text{diff},2} = L_0^2/D_2$. Since a bond connects two binders, in the simplest situation its mobility is half that of a free binder, hence $D_2 = 2 D_1$. With our choice of parameters, $\tau_{\text{diff},2} \approx 100 \tau_{\text{diff},1}$. Regarding reactions, the natural time scale is $\tau_{\text{reac}} = 1/\bar{k}_{\text{off}}$. Once \bar{k}_{off} is fixed, we determine the binding rate from $\bar{K}/c_0 = \bar{k}_{\text{on}}/\bar{k}_{\text{off}}$, which results from equations (2.1) and (2.3). The ratios between the reaction time scale and the diffusive time scales introduce Damkohler numbers weighing the relative importance of reactions and diffusion. For compliant bonds/binders, we consider a reference stiffness of $k = 2.5 \times 10^{-4} \text{ N m}^{-1}$.

3. Results

3.1. Diffusion-dominated regime

We first focused on the situation in which reactions are extremely slow compared with diffusion by setting \bar{k}_{on} and \bar{k}_{off} to zero and thus $\tau_{\text{reac}} = +\infty$. In this limit, the dynamics of free binders become uncoupled from the rest of the system. Thus, we are only left with one time scale associated with the diffusion of bonds. For a typical diffusion coefficient of free binders on lipid membranes, $D_2 = 2D_1 = 0.5 \mu\text{m}^2 \text{ s}^{-1}$, this time scale is $\tau_{\text{diff},1} \approx 25 \text{ s}$. We first considered non-compliant bonds by setting $h(s, t) = 0$; see electronic supplementary material, note 1. For this model, the state in figure 1a is an exact equilibrium state at $F=0$. We then suddenly applied a separation force F . We reasoned that, in response to force application, the contact angle should rapidly increase $\theta > \theta_0$, requiring a concomitant increase in bond concentration at the interface according to equation (2.10). In turn, this should create a sharp positive gradient in bond concentration and chemical potential, and hence a motion of the interface leading to patch shrinkage (equation (2.9)). As the patch becomes smaller, bond chemical potentials should equilibrate faster since they diffuse over a smaller distance and, since the number of bonds is constant, the patch should become increasingly concentrated with bonds. Our simulations confirmed this physical picture (figure 2a,b; electronic supplementary material, figure S1a,c and movie S1), and the system reaches a new equilibrium state where μ_1 is high and uniform and the higher bond osmotic tension balances the larger out-of-equilibrium membrane force at the interface

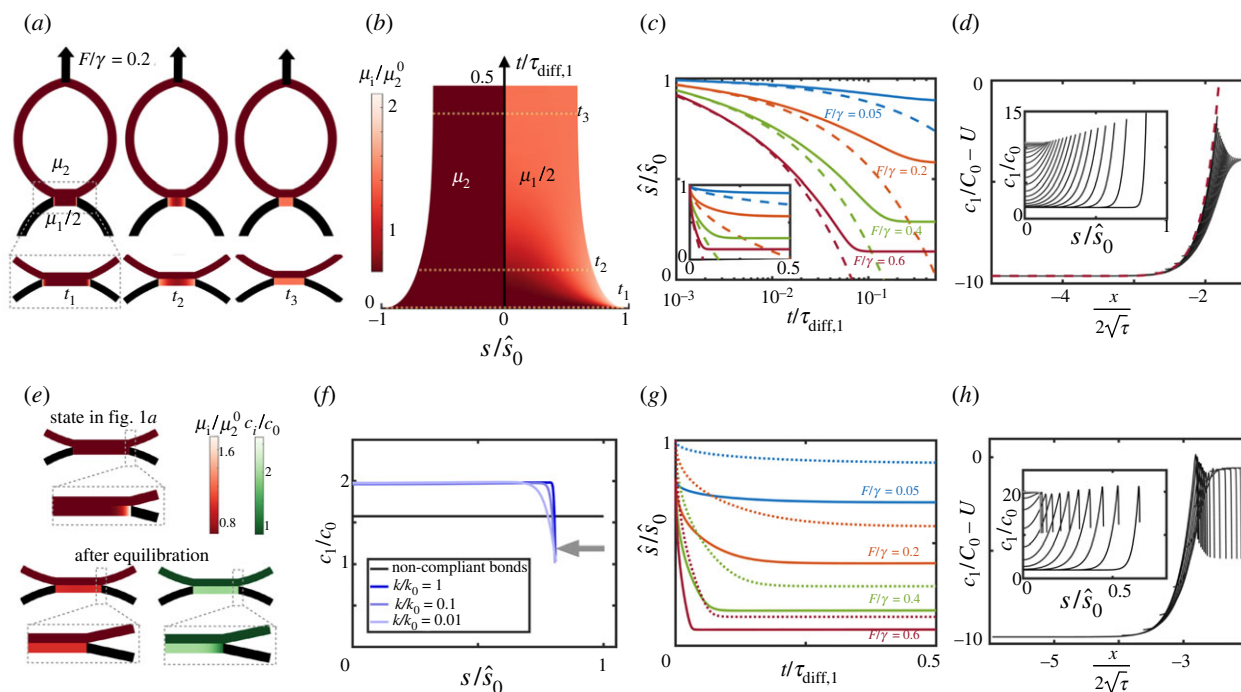


Figure 2. Diffusion-dominated regime for non-compliant (*a–d*) and compliant (*e–h*) bonds. (*a*) Snapshots of the shape of the adherent vesicles and the chemical potentials after application of $F/\gamma = 0.2$ with non-compliant bonds. (*b*) Kymograph of the interface position and chemical potentials of free binders (left) and bonds (right). (*c*) Position of the interface as a function of time for different applied forces. Dashed lines are the short-time analytical predictions in equation (3.2). The semi-logarithmic scale highlights the short-time behaviour; see inset for linear scale. (*d*) Bond concentration as a function of position at various instants (inset) and in terms of the similarity variable; the red dashed line is the analytical solution in equation (3.1). (*e*) The state in figure 1*a* is not in equilibrium for compliant bonds since stretching near the interface of the patch increases μ_1 . Upon equilibration μ_1 becomes uniform but cannot equilibrate with μ_2 in the absence of reactions, and c_1 has a boundary layer depleted of bonds. (*f*) Dependence of the equilibrium bond distribution and patch size on bond stiffness normalized by $k_0 = 2.5 \times 10^{-4} \text{ N m}^{-1}$. (*g*) Dynamics of the interface upon force application with compliant bonds; dotted lines indicate the interface dynamics for non-compliant bonds. In (*b,c,f,g*), \hat{s} is non-dimensionalized by the equilibrium size of the patch at $F = 0$ and non-compliant bonds. (*h*) Bond concentration for compliant bonds as a function of s (inset) and as a function of the similarity variable.

(equation (2.10)). Hence, the system is able self-adjust the effective adhesion fracture energy, $k_B T c_1(\hat{s}, t)$, to balance the higher peeling driving force. Although the final chemical potential of bonds is much larger than that of free binders, equilibration between species is not possible in the absence of reactions (figure 2*a,b*).

As F increases, θ also increases and a larger osmotic tension, and hence a larger bond concentration, is required to balance the mechanical force at the interface. Since the number of bonds is constant, this in turn requires a smaller equilibrium patch (electronic supplementary material, figure S1*b*, figure 2*c*). Interestingly, a similar process of shrinkage and concentration of adhesive patches has been observed in cell doublets under force *in vitro*, and during cell–cell hydraulic fracture in developing embryos [7,25].

Increasing the force also leads to faster dynamics (figure 2*c*; electronic supplementary material, movie S1). To further understand peeling dynamics, we sought an analytical solution. Starting from the equilibrium state in figure 1*a* with contact angle θ_0 , patch size \hat{s}_0 and uniform bond concentration $c_1(s, 0) = C_0 = 2\gamma(1 - \cos\theta_0)/(k_B T)$, we suddenly increased the force and hence $\theta > \theta_0$. In the actual system, as $\hat{s}(t)$ decreases so does $\theta(t)$ owing to vesicle capillarity (figure 2*d*, inset). To develop the analytical solution, we simplified the problem by assuming that θ remains constant during peeling. Introducing non-dimensional space $x = s/\hat{s}_0 - 1$, time $\tau = t/\tau_{\text{diff},1}$, driving parameter $U = (1 - \cos\theta)/(1 - \cos\theta_0)$, position of the interface $X(\tau) = \hat{s}(\tau_{\text{diff},1}\tau)/\hat{s}_0 - 1$ and concentration of bonds $u(x, \tau) = c_1(\hat{s}_0(x + 1), \tau_{\text{diff},1}\tau)/C_0 - U$, the governing equations (2.3),

(2.9) and (2.10) take the form of a classical Stefan problem; see electronic supplementary material, note 2, which describes a myriad of phase transformation problems [51]. This problem admits an analytical solution valid at short times or for large domains in terms of the similarity variable $x/\sqrt{\tau}$,

$$u(x, \tau) = \sqrt{\pi}\lambda e^{\lambda^2 U} \left[\text{erf}(\lambda) - \text{erf}\left(\frac{x}{2\sqrt{\tau}}\right) \right] \quad (3.1)$$

and

$$X(\tau) = 2\lambda\sqrt{\tau}, \quad (3.2)$$

where erf is the error function and λ is a constant depending on the driving parameter U and is implicitly determined by $\sqrt{\pi}\lambda e^{\lambda^2 U} [\text{erf}(\lambda) + 1] = 1 - U$. To linear order in $U - 1$, $\lambda(U) \approx -(U - 1)/\sqrt{\pi} \propto (\cos\theta - \cos\theta_0)$, showing how the interface motion depends on the horizontal force imbalance. Interestingly, the diffusion-controlled spreading of a membrane with mobile molecules binding to fixed receptors exhibits analogous self-similar dynamics [31,32].

We then compared these analytical predictions, valid at short times/large domains and assuming that θ remains constant, with our numerical calculations, which did not make any of these assumptions. At short times, equation (3.2) predicts very well the motion of the interface, particularly at high forces where the interface moves significantly before the finite-size effects leading to self-stabilization of the interface start to play a role (figure 2*c*). To further test the theory, we plotted the rescaled bond concentration at different time instants against the similarity variable, finding a remarkable

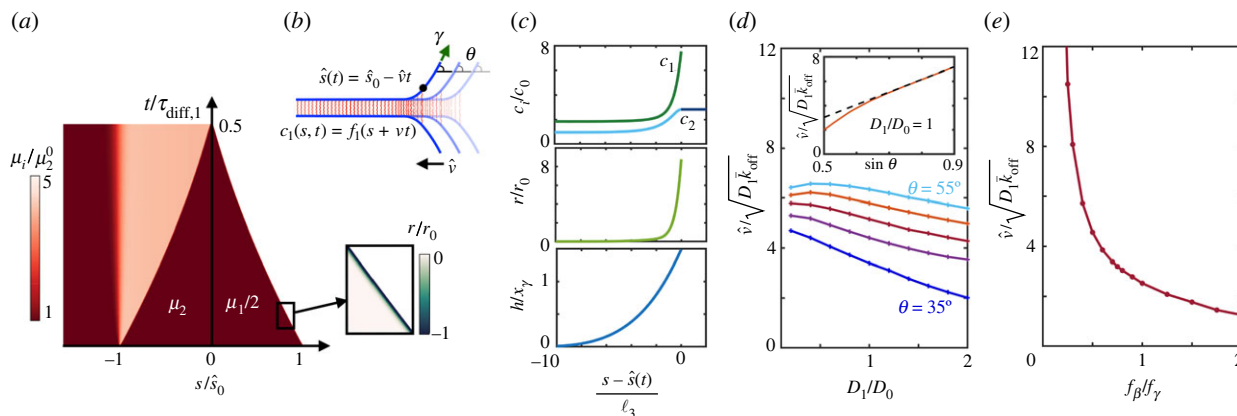


Figure 3. Reaction-dominated regime. (a) Kymograph of chemical potentials and net binding rate for $f_\beta/f_\gamma = 4$, $D_1/D_0 = 1$ and $F/\gamma = 0.5$ (inset), where $r_0 = \bar{k}_{\text{off}} c_0$. (b) Illustration of the travelling solution where θ is kept constant and (c) concentration, reaction rate and separation profiles for the travelling solution corresponding to $f_\beta/f_\gamma = 4$, $D_1/D_0 = 1$ and $\theta = 32^\circ$. (d) Velocity of the interface normalized by the prediction $v_0 = \sqrt{D_1 \bar{k}_{\text{off}}}$ as a function of diffusivity for $f_\beta/f_\gamma = 4$ and several contact angles θ . Normalized interface velocity as a function of $\sin\theta$ for $D_1/D_0 = 1$ (inset). (e) Normalized velocity of the interface as a function of force sensitivity for $D_1/D_0 = 1$ and $\theta = 32^\circ$.

collapse to equation (3.1) despite the reduction of θ with time and finite-size effects (figure 2d). These results thus establish a mapping between the dynamics of forced adhesions between membranes mediated by long-lived bonds and the self-similar solution of the classical Stefan problem.

Next, we examined numerically the more realistic situation of deformable bonds while keeping all other model parameters equal, including the total number of bonds. In this case, the state in figure 1a is not in equilibrium for $F=0$ since bonds are stretched in a boundary layer near the interface, which modifies their chemical potential (equation (2.6) and figure 2e). Despite the small size of the perturbed region, the new equilibrium state is significantly smaller and more concentrated (figure 2f; electronic supplementary material, figure S1c,d). The width of the boundary layer where bonds are stretched and depleted is commensurate with ℓ_2 and thus decreases with increasing bond stiffness, but the new position of the interface is quite insensitive to k (figure 2f). Interestingly, the results for non-compliant bonds are not the limit as $k \rightarrow +\infty$ of those for compliant bonds. We note, in this respect, that in this limit both h and x_γ tend to zero, and hence the last term in equation (2.6) does not necessarily tend to zero to recover the non-compliant case. Upon force application following equilibration, the dynamics proceed similarly to the case of non-compliant bonds, albeit at a faster rate (figure 2g; electronic supplementary material, figure S1c,d and movie S2). To understand the faster dynamics, we note that, close to the edge of the adhesion patch, the entropic and stretching components of the chemical potential of bonds (equation (2.6)) compete and become similar (electronic supplementary material, figure S1e), with bonds tending to move towards the depleted edge because of entropy and tending to move away from it to avoid stretching. During peeling, bond transport due to stretching dominates at the edge, driving inward interface motion (equation (2.9)). Thus, the effect of bond stretching is limited to a very small region close to the edge but has macroscopic effects in setting the equilibrium patch size and bond concentration and the kinetics of the peeling process. Although the similarity solution does not account for bond compliance, bond concentration at different times remarkably collapses when rescaled and plotted in the similarity variable (figure 2h), showing that the Stefan problem

captures the physics of this diffusion-dominated regime at short times.

We finally examined the force distribution in the adhesion patch. The out-of-plane traction $k c_1(s, t)h(s, t)$ needs to balance F and hence increases with it. However, increasing F does not lead to further separation. Instead, the system adapts to higher F (higher θ) by increasing $c_1(s, t)$ near the interface (equation (2.10)), while keeping a rather constant profile of the force per molecule, $kh(s, t)$, with a force scale emerging from the competition of mixing entropy and bond stretching (equation (2.6)) and given by $f_\gamma = \sqrt{k \cdot k_B T} \approx 1.0$ pN (electronic supplementary material, figure S2).

3.2. Reaction-dominated case

We then studied a different extreme scenario characterized by fast reaction rates, $\bar{k}_{\text{off}} = 10 \text{ s}^{-1}$, representative of weak bonds such as cadherins, and very low diffusivity, which should result in a reaction-dominated regime similar to the tear-out of an adhesive vesicle from a solid substrate with immobile receptors [28–30]. We decreased $D_{1,2}$ by a factor of about 1000 ($D_1 = D_2/2 = D_0 = 0.25 \times 10^{-3} \text{ } \mu\text{m}^2 \text{ s}^{-1}$), which is comparable to the reduction of diffusivity of adhesion molecules from artificial lipid bilayers to cell membranes [52], and initially considered rather insensitive slip bonds with $f_\beta/f_\gamma = 4$. Upon force application, we observed that, in contrast to the diffusion-dominated case where $\hat{s}(t) - \hat{s}_0 \propto \sqrt{t}$, now both the size of the patch and the number of bonds decrease nearly linearly, with the net unbinding reaction rate localized in close vicinity to the interface (figure 3a; electronic supplementary material, movie S3). Complete decohesion is reached before significant diffusion of bond or free binders can take place at the patch or vesicle scales.

In view of these results, we hypothesized the existence of travelling solutions of the form $c_i(s, t) = f_i(s + \hat{v}t)$ (figure 3b). To systematically examine this point, we again made the approximation of constant driving force (constant θ). Propagating fronts in reaction–diffusion systems requires non-generic nonlinearity, as in the prototypical Fisher–Kolmogorov–Petrovskii–Piscunov (FKPP) equation [53,54] or in the FitzHugh–Nagumo system [55]. For non-compliant ideal bonds, our model in the moving frame reduces to a two-species advection–reaction–diffusion equation whose only

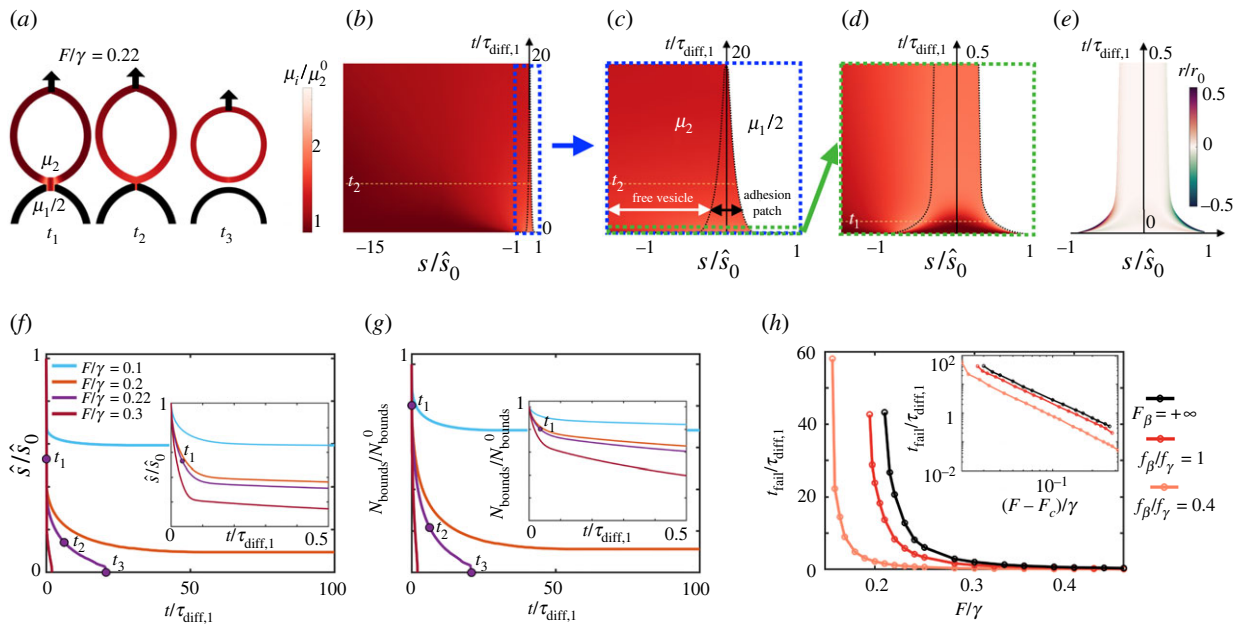


Figure 4. Mixed reaction–diffusion regime. (a) Snapshots of the shape of the adherent vesicles and of the chemical potentials after application of $F/\gamma = 0.22$ with compliant ideal bonds, leading to full decohesion. The three time instants are labelled in *b–g*. (b–d) Kymographs at different space and time scales of the position of the interface (dashed black line) and the chemical potential of free binders over the entire vesicle (left) and bonds over the patch (right). (e) Kymograph of the net rate of free binder (left) and bond (right) increase due to reactions. (f) Position of the interface and (g) number of bonds in the patch as a function of time for different applied forces. (h) Failure time as a function of applied force for ideal and for slip bonds.

nonlinearity is the term $\bar{k}_{\text{on}}c_2^2$, and our simulations did not develop travelling solutions. Instead, for compliant and force-sensitive bonds the model couples to mechanics, which predicts a separation profile h localized near the adhesion edge that in turn biases bond motion away from the edge, locally increases off rates and decrease on rates. In this case, our simulations readily developed travelling solutions with constant interface velocity, localized unbinding, a sharp transition of bonds to accommodate the concentration at $s = \hat{s}(t)$ (equation (2.10)) and a sharp transition of free binders to a higher plateau in the wake of the interface due to broken bonds (figure 3c; electronic supplementary material, figure S3).

To understand the physics controlling the peeling speed \hat{v} and the local profiles around $s = \hat{s}(t)$, we reasoned that, even though the time of bond diffusion in the whole patch is very long, $\tau_{\text{diff},1} \gg \tau_{\text{reac}}$, there should be a small length scale ℓ_3 over which diffusion and reactions compete near the interface, $\ell_3^2/D_1 \approx \tau_{\text{reac}}$, leading to $\ell_3 = \sqrt{D_1/\bar{k}_{\text{off}}} \approx 5$ nm. For our parameter set, ℓ_3 is smaller than ℓ_2 , over which bonds are loaded. Dimensional analysis and the analogy with the FKPP model suggest that this small-scale diffusion may control the overall decohesion process by setting the front speed $v_0 = \sqrt{D_1\bar{k}_{\text{off}}} \approx 50$ nm s⁻¹. This situation is also analogous to fracture mechanics of solids, where the physics within a small *process zone* in the vicinity of the crack tip determines the effective fracture properties [56]. Our simulations confirmed that v_0 and ℓ_3 provide order-of-magnitude estimates of peeling velocity and size of disturbed region (figure 3c,d).

However, the system exhibits a more complex behaviour that depends on a delicate interplay not only of bond transport and reactions but also of mechanics through h (equations (2.3), (2.7) and (2.8)). This interplay controls the dynamical organization in the moving process zone (electronic supplementary material, figure S3) and ultimately front velocity. As in the diffusion-dominated case, we

found that dynamics are faster for a larger mechanical driving force θ . However, here \hat{v} is nearly proportional to the vertical component of force ($\sin \theta$) (figure 3d, inset). We finally examined the influence of the slip bond effect, finding a very strong increase of \hat{v} as bonds became more sensitive to force, i.e. when f_β becomes smaller than the force scale close to the edge given by f_γ (figure 3e).

In summary, unlike the non-local and self-stabilizing peeling dynamics of the diffusion-dominated regime, here the front moves at a constant speed that depends only on the driving force and material parameters $\hat{v}(\theta; D_i, k, f_\beta, \bar{k}_{\text{off}}, \bar{k}_{\text{on}})$ akin to the kinetic law for the motion of a material interface [57]. The unconventional tear-out described here also differs from the classical tear-out for immobile bonds [15] in that it fundamentally depends not only on marginal unbinding but also on small-scale diffusion near the front.

3.3. Reaction–diffusion regime

To examine an intermediate regime, we kept the off-rate $\bar{k}_{\text{off}} = 10$ s⁻¹ representative of weak bonds such as cadherins and considered diffusion constants typical of adhesion molecules on lipid membranes, $D_2 = 2D_1 = 0.5$ μm^2 s⁻¹. In this regime, depending on the magnitude of the applied force, the adhesive patch can either fail or reach a stable configuration with full uniformization and equilibration of the chemical potentials of bonds and free binders (electronic supplementary material, movie S4). With our choice of \bar{k}_{off} , reactions take place much faster than diffusion, $\tau_{\text{reac}} \approx 0.1$ s $\ll \tau_{\text{diff},1} \approx 25$ s, and thus chemical potentials between bonds and free binders locally equilibrate very quickly in the adhesion patch (electronic supplementary material, figure S4a). For longer lived bonds, e.g. $\bar{k}_{\text{off}} = 0.1$ s⁻¹, reactions and diffusion dynamically compete (electronic supplementary material, figure S4b), leading to stronger

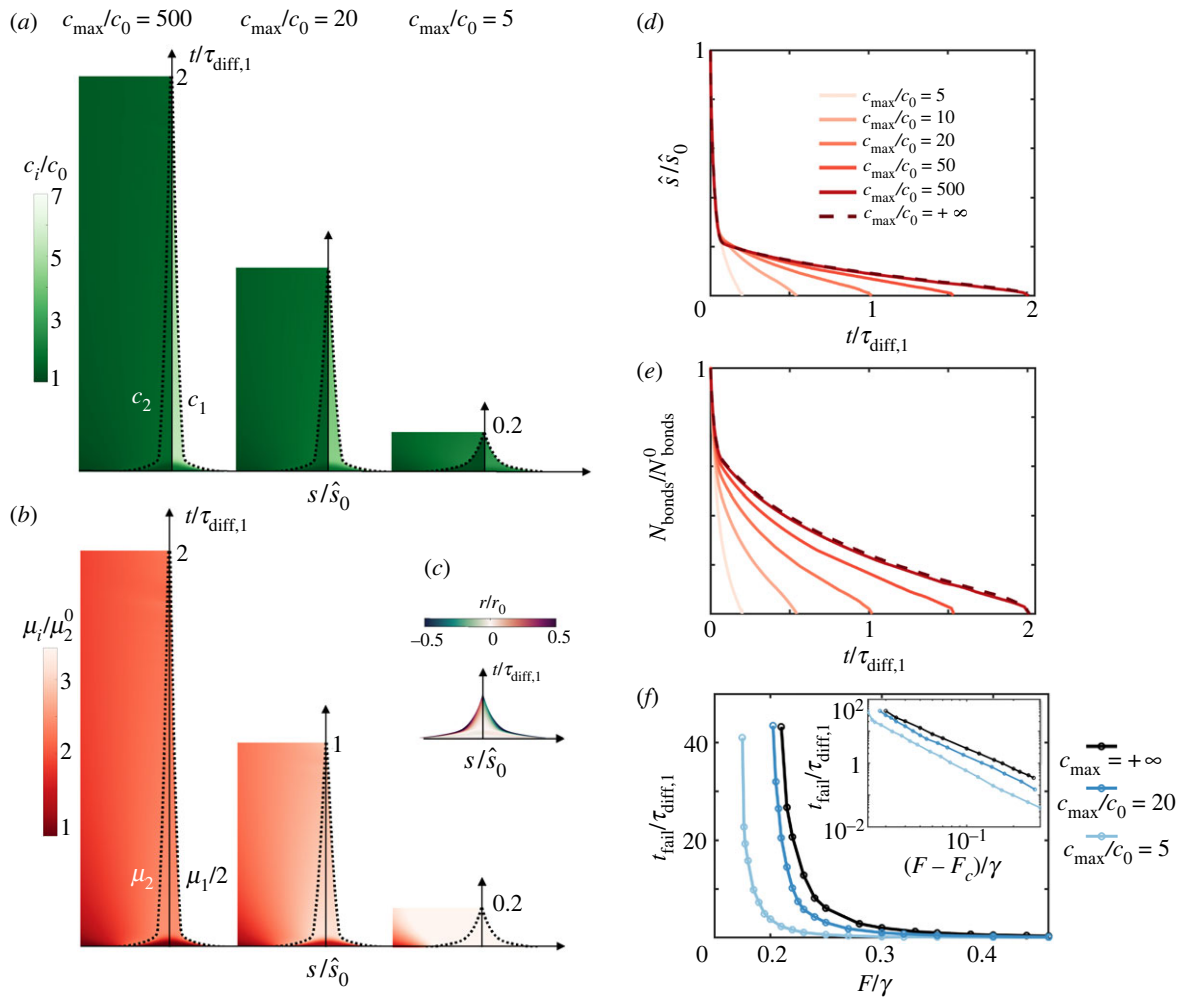


Figure 5. Effect of crowding in the mixed reaction–diffusion regime. Kymographs of concentrations (a) and of chemical potentials (b) in the vicinity of the adhesion patch for $F/\gamma = 0.3$, ideal bonds and three different degrees of crowding. Higher crowding corresponds to smaller c_{\max} , whereas $c_{\max}/c_0 = 500$ nearly coincides with the dilute limit $c_{\max} = +\infty$. (c) Kymograph of normalized reaction rate for the most crowded case. (d) Position of the interface and (e) number of bonds as a function of time and for different degrees of crowding and for the dilute limit $c_{\max} = +\infty$. (f) Failure time as a function of applied force for different degrees of crowding.

adhesions as a whole (electronic supplementary material, figure S4c,d).

Going back to the case of fast reaction rates ($\bar{k}_{\text{off}} = 10 \text{ s}^{-1}$) and first focusing on compliant ideal bonds ($f_{\beta} = +\infty$), we studied in detail the peeling dynamics, which exhibit multiple scales in space and time, as shown the kymographs (figure 4b–e). At short times commensurate with the diffusion time scale in the patch $\tau_{\text{diff},1}$, the dynamics proceed similarly to a self-similar diffusion-dominated regime (figure 4d,f, inset), but now, as in the reaction-dominated regime, fast unbinding localizes at the edge of the patch to reduce the chemical potential of stretched and concentrated bonds (figure 4e), leading to a fast initial decrease of the total number of bonds (figure 4g, inset). Examining early times, $t = t_1, t_2$, even if μ_1 and μ_2 equilibrate and uniformize within the adhesion patch, the local excess chemical potential of free binders μ_2 resulting from fast unbinding has not had time to equilibrate in the rest of the vesicle, driving diffusion of free binders away from the patch (figure 4a,b), thereby reducing μ_2 in the patch and further driving unbinding reactions (figure 4g). This process is much slower since it is controlled by the diffusive time scale over the vesicle, $\tau_{\text{diff},2} = 100\tau_{\text{diff},1}$. Since $\tau_{\text{diff},2} \gg \tau_{\text{diff},1} \gg \tau_{\text{reac}}$, now reactions take place nearly uniformly in a quasi-equilibrated adhesion patch. With fewer bonds, mechanical equilibrium at the interface requires reducing the size of the patch, which

decreases the contact angle and increases bond concentration (equation (2.10)). In turn, the higher bond concentration favours further unbinding. Thus, the much slower dynamics during this second phase are complex, multi-phasic and depend on the diffusion of free binders over the entire vesicle with time scale $\tau_{\text{diff},2}$ (figure 4f,g).

The speed and outcome of these dynamics depend on the magnitude of F . To characterize adhesion strength, we simulated the dynamics for different forces and tracked the time to complete failure t_{fail} (figure 4h), finding that lifetime very abruptly increases as force is reduced [36]. This suggests the existence of a threshold force below which the patch is long-lived and above which decohesion occurs rapidly. Consistent with this, lifetime closely follows a power law $t \propto (F - F_c)^a$ with $a \approx -2.2$ and the critical force F_c a fitting parameter (figure 4h, inset). Thus, F_c can be interpreted as the strength of the adhesion patch. This mesoscopic notion of strength should depend on the microscopic strength of individual bonds given by f_{β} . As in the FKPP regime, we found that force sensitivity of slip bonds only plays a significant role when $f_{\beta} < f_{\gamma}$, in which case lifetime at fixed F and strength dramatically reduce (figure 4h).

Up to now, our model assumes a dilute limit of molecules on the membrane. However, force application leads to increasing molecular crowding, which should affect the

dynamics of decohesion by changing the interplay between reactions and diffusion. Crowding has been shown to facilitate passive endocytosis of particles with mobile binders [58] and to modify the mechanisms and morphology of nascent adhesions [59]. We thus developed a model accounting for crowding by considering a more general expression for the mixing entropy based on the Flory–Huggins theory that included cross-diffusion effects (electronic supplementary material, note 1). According to this model, close to a maximum concentration of molecules, c_{\max} , the chemical potential of bonds

$$\mu_1 = \mu_1^0 + k_B T \frac{c_1}{c_0} - 2k_B T \log\left(\frac{c_{\max} - c_1 - c_2}{c_{\max}}\right) + k_B T \left(\frac{h}{x_\gamma}\right)^2 \quad (3.3)$$

rapidly increases, which accelerates unbinding reactions and increases the effective diffusion coefficient. Close to the crowding limit, the osmotic tension of bonds takes the form $-k_B T (2c_{\max} \log[(c_{\max} - c_1)/c_{\max}] + c_1)$, which blows up as $c_1 \rightarrow c_{\max}$ and reduces to the van't Hoff form $k_B T c_1$ used before in the dilute limit $c_1 \ll c_{\max}$. For high crowding ($c_{\max}/c_0 = 5$), our simulations show that concentrations uniformize much more rapidly than in the dilute limit and to a lower value as saturation is reached in the patch (figure 5a). The patch rapidly shrinks until failure because of unbinding reactions taking place throughout the adhesion driven by the higher chemical potential of bonds in a crowded situation (figure 5b–e). Systematic simulations at various forces show that crowding accelerates failure and reduces F_c analogously to the effect of slip bond sensitivity (figure 5f). Hence, crowding weakens the adhesion patch by favouring a tear-out mechanism with diffuse unbinding (figure 5c), different from the FKPP regime exhibiting highly localized marginal unbinding (figure 3a). For cadherins on lipid vesicles, $c_{\max}/c_0 \approx 20$ [60], our model still predicts significant weakening caused by crowding relative to the dilute limit. Our analysis does not include the effect of other membrane molecules, which can act as crowders but not contribute to adhesion.

4. Summary and discussion

In summary, we have developed an out-of-equilibrium model self-consistently coupling diffusion, binding and unbinding reactions and mechanics to understand the dynamics of peeling between fluid membranes bridged by mobile adhesion molecules forming transient bonds. We have used this model to map various distinct and biologically relevant scenarios of forced decohesion amenable to experimental examination. In all of these scenarios, the macroscopic peeling behaviour depends on the physics occurring in a very small *process zone* close to the edge of the adhesion patch. (i) For long-lived mobile bonds, adhesion patches shrink and become concentrated in a self-stabilizing process controlled by diffusion. At short times, the system evolves

according to the self-similar dynamics of a classical Stefan problem with the interface moving as $(\hat{s}(t) - \hat{s}_0) \propto \sqrt{t}$. (ii) For short-lived bonds with low diffusivity, such as cadherins partially immobilized by the cytoskeleton, we have identified a new unconventional tear-out regime characterized by FKPP-like travelling solutions with $(\hat{s}(t) - \hat{s}_0) \propto t$, which are localized reactions in the vicinity of the interface, but also by small-scale diffusion in a process zone of size $\sqrt{D_1/\bar{k}_{\text{off}}}$. The interplay between diffusion and reactions sets the order of magnitude of the front speed $\sqrt{D_1 \bar{k}_{\text{off}}}$, but this speed is strongly influenced by the applied force and by the ratio between force sensitivity f_β and the characteristic force born by bonds close to the interface $f_\gamma = \sqrt{k \cdot k_B T}$. (iii) For mobile short-lived bonds such as cadherins on a lipid membrane, the system exhibits a hierarchy of reaction and diffusion time scales resulting in multi-phasic dynamics. The reinforcing effect of bond motion and the weakening effect of bond breaking compete in a force-dependent manner, defining the strength of the patch below which peeling arrests and above which peeling rapidly leads to complete failure. Strength strongly decreases for sensitive bonds ($f_\beta < \sqrt{k \cdot k_B T}$) and with molecular crowding.

Although our minimal model ignores important aspects of cell–cell adhesion, the physical rules identified here should bear biological relevance. We have shown how the ability of bonds to laterally move in fluid–fluid adhesive interfaces leads to a very rich repertoire of peeling scenarios that cells can use to stabilize cell–cell junctions during physiological stretch, or to selectively detach during morphogenesis. For instance, cells can effectively tune adhesive strength, and hence their ability to stay adhered or to disengage, by controlling molecular properties of bonds such as stiffness k and force sensitivity f_β e.g. through extracellular Ca^{2+} , by controlling the number of transmembrane crowding molecules or by controlling the actively generated surface tension. Beyond cells, our study also provides a conceptual framework for artificial biomimetic systems with a comparable degree of adhesive tunability [45].

Data accessibility. The Matlab computer codes used to generate the results in the manuscript are available from: https://github.com/pradeep927/Peeling_dynamics_matlab.git.

The data are provided in the electronic supplementary material [61].

Authors' contributions. D.K.: conceptualization, investigation, methodology, software; P.K.B.: investigation, methodology, software; M.A.: conceptualization, funding acquisition, investigation, project administration, software, supervision, writing—original draft.

All authors gave final approval for publication and agreed to be held accountable for the work performed herein.

Conflict of interest declaration. We declare we have no competing interest.

Funding. The authors acknowledge the support of the European Research Council (CoG-681434), the European Commission (project no. H2020-FETPROACT-01-2016-731957), the Spanish Ministry for Science and Innovation (PID2019-110949GB-I00) and the Generalitat de Catalunya (2017-SGR-1278 and ICREA Academia prize for excellence in research). IBEC and CIMNE are recipients of a Severo Ochoa Award of Excellence from the MINECO.

References

- Harris AR, Peter L, Bellis J, Baum B, Kabla AJ, Charras GT. 2012 Characterizing the mechanics of cultured cell monolayers. *Proc. Natl Acad. Sci. USA* **109**, 16 449–16 454. (doi:10.1073/pnas.1213301109)
- Casares L, Vincent R, Zalvidea D, Campillo N, Navajas D, Arroyo M, Trepast X. 2015 Hydraulic

- fracture during epithelial stretching. *Nat. Mater.* **14**, 343–351. (doi:10.1038/nmat4206)
3. Latorre E *et al.* 2018 Active superelasticity in three-dimensional epithelia of controlled shape. *Nature* **563**, 203–208. (doi:10.1038/s41586-018-0671-4)
 4. Friedl P, Alexander S. 2011 Cancer invasion and the microenvironment: plasticity and reciprocity. *Cell* **147**, 992–1009. (doi:10.1016/j.cell.2011.11.016)
 5. Lecuit T, Lenne P-F. 2007 Cell surface mechanics and the control of cell shape, tissue patterns and morphogenesis. *Nat. Rev. Mol. Cell Biol.* **8**, 633–644. (doi:10.1038/nrm2222)
 6. Guillot C, Lecuit T. 2013 Mechanics of epithelial tissue homeostasis and morphogenesis. *Science* **340**, 1185–1189. (doi:10.1126/science.1235249)
 7. Dumortier JG, Le Verge-Serandour M, Tortorelli AF, Mielke A, de Plater L, Turlier H, Maître J-L. 2019 Hydraulic fracturing and active coarsening position the lumen of the mouse blastocyst. *Science* **365**, 465–468. (doi:10.1126/science.aaw7709)
 8. Tetley RJ, Staddon MF, Heller D, Hoppe A, Banerjee S, Mao Y. 2019 Tissue fluidity promotes epithelial wound healing. *Nat. Phys.* **15**, 1195–1203. (doi:10.1038/s41567-019-0618-1)
 9. Bell G, Dembo M, Bongrand P. 1984 Cell adhesion. Competition between nonspecific repulsion and specific bonding. *Biophys. J.* **45**, 1051–1064. (doi:10.1016/S0006-3495(84)84252-6)
 10. Yap AS, Gomez GA, Parton RG. 2015 Adherens junctions revisualized: organizing cadherins as nanoassemblies. *Dev. Cell* **35**, 12–20. (doi:10.1016/j.devcel.2015.09.012)
 11. Yap AS, Duszyc K, Viasnoff V. 2017 Mechanosensing and mechanotransduction at cell–cell junctions. *Cold Spring Harbor Perspect. Biol.* **10**, a028761. (doi:10.1101/cshperspect.a028761)
 12. Maître J-L, Heisenberg C-P. 2013 Three functions of cadherins in cell adhesion. *Curr. Biol.* **23**, R626–R633. (doi:10.1016/j.cub.2013.06.019)
 13. Cai Y, Shashikanth N, Leckband DE, Schwartz DK. 2016 Cadherin diffusion in supported lipid bilayers exhibits calcium-dependent dynamic heterogeneity. *Biophys. J.* **111**, 2658–2665. (doi:10.1016/j.bpj.2016.10.037)
 14. Rakshit S, Zhang Y, Manibog K, Shafraz O, Sivasankar S. 2012 Ideal, catch, and slip bonds in cadherin adhesion. *Proc. Natl Acad. Sci. USA* **109**, 18 815–18 820. (doi:10.1073/pnas.1208349109)
 15. Dembo M, Torney DC, Saxman K, Hammer D. 1988 The reaction-limited kinetics of membrane-to-surface adhesion and detachment. *Proc. R. Soc. B* **234**, 55–83.
 16. Brochard-Wyart F, de Gennes P-G. 2002 Adhesion induced by mobile binders: dynamics. *Proc. Natl Acad. Sci. USA* **99**, 7854–7859. (doi:10.1073/pnas.112221299)
 17. de Gennes P-G, Puech P-H, Brochard-Wyart F. 2003 Adhesion induced by mobile stickers: a list of scenarios. *Langmuir* **19**, 7112–7119. (doi:10.1021/la034421g)
 18. Albersdörfer A, Feder T, Sackmann E. 1997 Adhesion-induced domain formation by interplay of long-range repulsion and short-range attraction force: a model membrane study. *Biophys. J.* **73**, 245–257. (doi:10.1016/S0006-3495(97)78065-2)
 19. Zhu C. 2000 Kinetics and mechanics of cell adhesion. *J. Biomech.* **33**, 23–33. (doi:10.1016/S0021-9290(99)00163-3)
 20. Nam J, Santore MM. 2007 The adhesion kinetics of sticky vesicles in tension: the distinction between spreading and receptor binding. *Langmuir* **23**, 10 650–10 660. (doi:10.1021/la7017709)
 21. Smith A-S, Sengupta K, Goennenwein S, Seifert U, Sackmann E. 2008 Force-induced growth of adhesion domains is controlled by receptor mobility. *Proc. Natl Acad. Sci. USA* **105**, 6906–6911. (doi:10.1073/pnas.0801706105)
 22. Sackmann E, Smith A-S. 2014 Physics of cell adhesion: some lessons from cell-mimetic systems. *Soft Matter* **10**, 1644. (doi:10.1039/c3sm51910d)
 23. Schmid EM, Bakalar MH, Choudhuri K, Weichsel J, Ann HS, Geissler PL, Dustin ML, Fletcher DA. 2016 Size-dependent protein segregation at membrane interfaces. *Nat. Phys.* **12**, 704–711. (doi:10.1038/nphys3678)
 24. Fenz SF, Bihl R, Schmidt D, Merkel R, Seifert U, Sengupta K, Smith A-S. 2017 Membrane fluctuations mediate lateral interaction between cadherin bonds. *Nat. Phys.* **13**, 906. (doi:10.1038/nphys4138)
 25. Maître J-L, Berthoumieux H, Krens SFG, Salbreux G, Jülicher F, Paluch E, Heisenberg C-P. 2012 Adhesion functions in cell sorting by mechanically coupling the cortices of adhering cells. *Science* **338**, 253–256. (doi:10.1126/science.1225399)
 26. Evans EA. 1985 Detailed mechanics of membrane-membrane adhesion and separation: I. Continuum of molecular cross bridges. *Biophys. J.* **48**, 175–183. (doi:10.1016/S0006-3495(85)83770-X)
 27. Evans EA. 1985 Detailed mechanics of membrane-membrane adhesion and separation. II. Discrete kinetically trapped molecular cross-bridges. *Biophys. J.* **48**, 185–192. (doi:10.1016/S0006-3495(85)83771-1)
 28. Berk D, Evans E. 1991 Detachment of agglutinin-bonded red blood cells. III. Mechanical analysis for large contact areas. *Biophys. J.* **59**, 861–872. (doi:10.1016/S0006-3495(91)82298-6)
 29. Pierrat S, Brochard-Wyart F, Nassoy P. 2004 Enforced detachment of red blood cells adhering to surfaces: statics and dynamics. *Biophys. J.* **87**, 2855–2869. (doi:10.1529/biophysj.104.043695)
 30. Lin Y, Freund LB. 2007 Forced detachment of a vesicle in adhesive contact with a substrate. *Int. J. Solids Struct.* **44**, 1927–1938. (doi:10.1016/j.ijsolstr.2006.09.006)
 31. Freund LB, Lin Y. 2004 The role of binder mobility in spontaneous adhesive contact and implications for cell adhesion. *J. Mech. Phys. Solids* **52**, 2455–2472. (doi:10.1016/j.jmps.2004.05.004)
 32. Shenoy V, Freund L. 2005 Growth and shape stability of a biological membrane adhesion complex in the diffusion-mediated regime. *Proc. Natl Acad. Sci. USA* **102**, 3213–3218. (doi:10.1073/pnas.0500368102)
 33. Gao H, Shi W, Freund LB. 2005 Mechanics of receptor-mediated endocytosis. *Proc. Natl Acad. Sci. USA* **102**, 9469–9474. (doi:10.1073/pnas.0503879102)
 34. Erdmann T, Schwarz US. 2007 Impact of receptor-ligand distance on adhesion cluster stability. *Eur. Phys. J. E* **22**, 123–137. (doi:10.1140/epje/e2007-00019-8)
 35. Gao H, Qian J, Chen B. 2011 Probing mechanical principles of focal contacts in cell-matrix adhesion with a coupled stochastic-elastic modelling framework. *J. R. Soc. Interface* **8**, 1217–1232. (doi:10.1098/rsif.2011.0157)
 36. Kaurin D, Arroyo M. 2019 Surface tension controls the hydraulic fracture of adhesive interfaces bridged by molecular bonds. *Phys. Rev. Lett.* **123**, 228102. (doi:10.1103/PhysRevLett.123.228102)
 37. Evans E, Leung A. 1984 Adhesivity and rigidity of erythrocyte membrane in relation to wheat germ agglutinin binding. *J. Cell Biol.* **98**, 1201–1208. (doi:10.1083/jcb.98.4.1201)
 38. Tozere A, Sung KL, Chien S. 1989 Theoretical and experimental studies on cross-bridge migration during cell disaggregation. *Biophys. J.* **55**, 479–487. (doi:10.1016/S0006-3495(89)82841-3)
 39. Maître J-L, Berthoumieux H, Krens SFG, Salbreux G, Jülicher F, Paluch E, Heisenberg C-P. 2012 Adhesion functions in cell sorting by mechanically coupling the cortices of adhering cells. *Science* **338**, 253–256.
 40. Zhu C. 1991 A thermodynamic and biomechanical theory of cell adhesion Part I: general formalism. *J. Theor. Biol.* **150**, 27–50. (doi:10.1016/S0022-5193(05)80473-4)
 41. Biswas KH. 2020 Molecular mobility-mediated regulation of e-cadherin adhesion. *Trends Biochem. Sci.* **45**, 163–173. (doi:10.1016/j.tibs.2019.10.012)
 42. Moggetti BM, Cicuta P, Michele L. 2019 Programmable interactions with biomimetic DNA linkers at fluid membranes and interfaces. *Rep. Prog. Phys.* **82**, 116601. (doi:10.1088/1361-6633/ab37ca)
 43. Xu G-K, Hu J, Lipowsky R, Weikl TR. 2015 Binding constants of membrane-anchored receptors and ligands: a general theory corroborated by Monte Carlo simulations. *J. Chem. Phys.* **143**, 243136. (doi:10.1063/1.4936134)
 44. Evans E. 1991 Entropy-driven tension in vesicle membranes and unbinding of adherent vesicles. *Langmuir* **7**, 1900–1908. (doi:10.1021/la00057a014)
 45. Parolini L, Moggetti BM, Kotar J, Eiser E, Cicuta P, Di Michele L. 2015 Volume and porosity thermal regulation in lipid mesophases by coupling mobile ligands to soft membranes. *Nat. Commun.* **6**, 5948. (doi:10.1038/ncomms6948)
 46. Carlson A, Mahadevan L. 2015 Protein mediated membrane adhesion. *Phys. Fluids* **27**, 051901. (doi:10.1063/1.4919777)
 47. Hu J, Xu G-K, Lipowsky R, Weikl TR. 2015 Binding kinetics of membrane-anchored receptors and ligands: molecular dynamics simulations and theory. *J. Chem. Phys.* **143**, 243137. (doi:10.1063/1.4936135)

48. Manibog K, Li H, Rakshit S, Sivasankar S. 2014 Resolving the molecular mechanism of cadherin catch bond formation. *Nat. Commun.* **5**, 3941. (doi:10.1038/ncomms4941)
49. Bell GI. 1978 Models for the specific adhesion of cells to cells. *Science* **200**, 618–627. (doi:10.1126/science.347575)
50. Rivlin RS. 1944 The effective work of adhesion. *Paint Technol.* **9**, 215.
51. Gupta SC. 2018 *The classical stefan problem*. Amsterdam, The Netherlands: Elsevier.
52. Biswas KH *et al.* 2015 E-cadherin junction formation involves an active kinetic nucleation process. *Proc. Natl Acad. Sci. USA* **112**, 10 932–10 937. (doi:10.1073/pnas.1513775112)
53. Kolmogorov A, Petrovskii I, Piscunov N. 1937 A study of the equation of diffusion with increase in the quantity of matter, and its application to a biological problem. *Byul. Moskovskogo Gos. Univ.* **1**, 1–25.
54. Fisher R. 1937 The wave of advance of advantageous genes. *Ann. Eugenics* **7**, 353.
55. Rinzel J, Keller JB. 1973 Traveling wave solutions of a nerve conduction equation. *Biophys. J.* **13**, 1313–1337. (doi:10.1016/S0006-3495(73)86065-5)
56. Tvergaard V, Hutchinson JW. 1992 The relation between crack growth resistance and fracture process parameters in elastic-plastic solids. *J. Mech. Phys. Solids* **40**, 1377–1397. (doi:10.1016/0022-5096(92)90020-3)
57. Abeyaratne R, Knowles JK. 2006 *Evolution of phase transitions*. New York, NY: Cambridge University Press.
58. Di Michele L, Jana PK, Moggetti BM. 2018 Steric interactions between mobile ligands facilitate complete wrapping in passive endocytosis. *Phys. Rev. E* **98**, 032406. (doi:10.1103/PhysRevE.98.032406)
59. Schmidt D, Bihl T, Fenz S, Merkel R, Seifert U, Sengupta K, Smith AS. 2015 Crowding of receptors induces ring-like adhesions in model membranes. *Biochim. Biophys. Acta* **1853**, 2984–2991. (doi:10.1016/j.bbamcr.2015.05.025)
60. Pontani L-L, Jorjadze I, Brujic J. 2016 Cis and trans cooperativity of e-cadherin mediates adhesion in biomimetic lipid droplets. *Biophys. J.* **110**, 391–399. (doi:10.1016/j.bpj.2015.11.3514)
61. Kaurin D, Bal PK, Arroy M. 2022 Peeling dynamics of fluid membranes bridged by molecular bonds: moving or breaking. Figshare. (doi:10.6084/m9.figshare.c.6039045)